Lab on a Chip

PAPER

View Article Online
View Journal | View Issue

Cite this: *Lab Chip*, 2017, **17**, 1505

Power-free, digital and programmable dispensing of picoliter droplets using a Digit Chip†

A. Mepham,[a] J. D. Besant,[a] A. W. Weinstein,[b] I. B. Burgess,[c] E. H. Sargent*[d] and S. O. Kelley*[ace]

There is a growing need for power-free methods to manipulate small volumes of liquids and thereby enable use of diagnostic assays in resource-limited settings. Most existing self-powered devices provide analog manipulation of fluids using paper, capillary or pressure-driven pumps. These strategies are well-suited to manipulating larger micro- and milliliter-scale volumes at constant flow rates; however, they fail to enable the manipulation of nanoliter and picoliter volumes required in assays using droplets, capillary sampling (*e.g.* finger prick), or expensive reagents. Here we report a device, termed the Digit Chip, that provides programmable and power-free digital manipulation of sub-nanoliter volumes. The device consists of a user-friendly button interface and a series of chambers connected by capillary valves that serve as digitization elements. *Via* a button press, the user dispenses and actuates ultra-small, quantitatively-programmed volumes. The device geometry is optimized using design models and experiments and precisely dispenses volumes as low as 21 pL with 97% accuracy. The volume dispensed can be tuned in 10 discrete steps across one order-of-magnitude with 98% accuracy. As a proof-of-principle that nanoliter-scale reagents can be precisely actuated and combined on-chip, we deploy the device to construct a precise concentration gradient with 10 discrete concentrations. Additionally, we apply this device alongside an inexpensive smartphone-based fluorescence imaging platform to perform a titration of *E. coli* with ampicillin. We observe the onset of bacterial death at a concentration of 5 μg mL^{-1}, increasing to a maximum at 50 μg mL^{-1}. These results establish the utility of the Digit Chip for diagnostic applications in low-resource environments.

Received 26th February 2017,
Accepted 14th March 2017

DOI: 10.1039/c7lc00199a

rsc.li/loc

Introduction

Despite recent advances in microfluidics for diagnostics, many of the most sensitive tests remain unavailable in resource-limited settings due to the prohibitive cost and power requirements of the necessary instrumentation.[1] Most microfluidic systems require costly electrically-powered pumps for fluidic actuation, and this limits the deployment of these technologies in the challenging field conditions of developing world environments, where in many cases the requirements of portability and remote location may limit access to reliable sources of electric power.

To increase access to point-of-care diagnostic technologies, low-cost and low-power fluidic actuation systems are needed.[1,2] Recently, compelling strategies for passive fluid control have been reported that have included lateral flow paper microfluidics,[3–5] vacuum pumps,[6,7] pressure pumps,[8,9] fibres,[10] and capillary pumps.[11,12] Sophisticated sample manipulations are possible using these power-free actuation systems, and multi-step assays have been demonstrated.[6,13–17] However, these analog approaches to fluid manipulation are typically optimized to regulate the flow rate of bulk fluids, and have not yet been demonstrated to be well-suited for complex manipulations of very small reagent volumes.

Many diagnostic assays require the use of small samples or reagent volumes, including those that sample blood from a finger prick and those that require expensive reagents. As a result, several chip-based techniques for digital manipulation of small volumes have been developed including droplet[18–20] and digital microfluidics.[21–23] In both cases, droplet actuation requires a power source such as an electric pump (droplet microfluidics) or a high voltage source (digital microfluidics). These requirements limit the feasibility of these methods in resource-limited environments.

Developing power-free platforms for digital manipulation of small sample volumes poses two distinct challenges not present in their analog counterparts: 1) dispensing

[a] *Institute for Biomaterials and Biomedical Engineering, University of Toronto, Toronto, ON, M5S 3G9, Canada. E-mail: shana.kelley@utoronto.ca*
[b] *Faculty of Engineering, University of Waterloo, Waterloo, ON, N2L 3G1, Canada*
[c] *Department of Pharmaceutical Sciences, Leslie Dan Faculty of Pharmacy, University of Toronto, Toronto, ON, M5S 3M2, Canada*
[d] *Department of Electrical and Computer Engineering, Faculty of Engineering, University of Toronto, Toronto, ON, M5S 3G4, Canada*
[e] *Department of Biochemistry, Faculty of Medicine, University of Toronto, Toronto, ON, M5S 1A8, Canada*

† Electronic supplementary information (ESI) available. See DOI: 10.1039/c7lc00199a

mechanisms need to be very precise and optimized for small volumes;[24,25] 2) sample controls need to be modular and compatible with a user-friendly interface. Innovative architectures for self-powered,[3] or manually-powered[26] fluid manipulation, including the SlipChip[27–30] have recently overcome a number of key challenges; however, thus far these self-powered techniques only allow a limited number of sequential manipulations and lack the modularity and programmability of powered techniques such as digital microfluidics. Devices driven by finger pressing have also been developed,[31,32] however, these devices typically make use of one directional flow valves and as such are considerably more difficult to manufacture. Moreover, these devices cannot manipulate picoliter volumes of fluid. Finally, these devices typically metre only a single, fixed volume of fluid.

Here, we develop a user-friendly interface for power-free and digital manipulation of small volumes using capillary-valve-dispensers as modular elements, which are linked to pressure-regulated buttons. The device, termed the Digit Chip, uses the pressure applied from pressing buttons manually to break individual capillary valves and move liquids in fixed-volume increments. Using theory and experiments, we optimize the geometry and surface properties of the valves and pressure-regulated buttons, and show that droplets can be dispensed and manipulated accurately across a wide range of volumes down to the picolitre scale. Dispensing, actuating, and mixing reagents are essential components of many important biological and chemical assays. To demonstrate that small volumes can be precisely actuated and mixed, we use the Digit Chip to create a precise, discretized concentration gradient with nanoliter volumes. We also illustrate how this architecture enables a convenient and low-cost technique to measure the susceptibility of bacteria to antibiotics. This is an important capability that could allow small collections of bacteria to be assessed for drug resistance *via* phenotypic testing without the need for any type of traditional lab infrastructure. The Digit Chip could also be applied in a variety of biological and chemical assays which depend on reagent dilutions and chemical gradients including generation of standard curves, optimization of reaction conditions,[33] and chemotaxis.[34]

Experimental

Digit Chip fabrication

Using standard photolithography, we patterned a 50 μm tall SU-8 3050 (Microchem, MA) layer on a silicon wafer (University Wafer, MA). PDMS (Dow Chemical, MI) was dispensed onto the wafer and cured for 1 hour at 67 °C. After curing, the PDMS was removed from the silicon wafer and holes were punched to form the inlet and outlet.

Fabrication of user-friendly interface

The mold was printed using a μPrint 3D printer. PDMS was dispensed onto the mold and cured at 67 °C for 1 hour. The PDMS was removed and holes were punched to create outlets and a small vent in the button chamber. The PDMS was plasma treated and bonded to a glass slide. Silicone tubing was used to attach the button to the Digit Chip.

Contact angle measurements

PDMS was treated with an oxygen plasma for a variety of exposure times. Advancing contact angles were measured using ImageJ to analyse images of the droplets acquired using a camera.

Bursting pressure measurements

Valve bursting pressures were measured using a syringe pump connected to the chip. After introducing PBS (pH 7.4) into the Digit Chip, the syringe pump was connected to the chip with 9.5 cm of silicone tubing (0.76 mm inner diameter). The initial volume of gas in the 1 mL syringe and tubing was measured. The syringe was slowly compressed at a rate of 20–50 μL min^{-1} while monitoring the capillary valve under a microscope. The pump was stopped and the pressure was relieved as soon as the valve burst. The volume change of gas contained in the syringe and tubing was recorded. The induced pressure was calculated using the initial and final volumes using the ideal gas law. The changes in pressure were measured at least 5 times per chip.

Measurements of applied pressure using the elastomeric button

The outlet of the user-interface was connected to silicone tubing (0.76 mm inner diameter) filled with a plug of PBS buffer (pH 7.4). After compressing the button, we recorded the change in displacement of the plug. This change in displacement of the plug was used to calculate the volume of gas displaced while pressing the button. This volume change was converted into a pressure change using Boyle's law.

Chamber filling percentage measurements

The filling percentage of chambers was measured by acquiring optical images under a microscope (Nikon) and analyzing the images using ImageJ.

Generation of a discretized concentration gradient

The device was fabricated from PDMS as stated above. Auxiliary air outlets were connected to each fluid inlet to enable fluid to be pumped in from both sides. Screw valves were fabricated on each air outlet by 3D printing a chuck to suspend the screws above the channel. The valves were closed or opened by turning the screw clockwise or counter-clockwise. Before dispensing the dyes, the air channels were blocked by closing the valves to ensure that liquid did not enter the air channels. Both samples were introduced and dispensed for the desired number of chambers. The sum of the number chambers filled with blue and yellow dyes was held constant at 10 for all concentrations. Samples used were ddH_2O with food coloring at 2 drops per mL. Devices were not plasma

treated or bonded to allow them to be reusable so 20% EtOH was added to the solutions to lower the contact angle. To prevent leakage, the channels were held against the substrate under light pressure. After dispensing, the valve was removed. Using a 1 mL syringe, air was injected by hand to move the droplets to the middle chamber. Mixing was aided by pressing on the middle chamber 3 times. Using an optical microscope, a picture of the mixed sample was recorded. The ratio of the dye was measured using ImageJ by recording the intensity of the dye and comparing it to the intensity of a bulk solution of dye mixed using standard laboratory pipettes and injected into the on-chip mixing chamber.

Antibiotic susceptibility testing

The device was fabricated in PDMS as stated above. Ampicillin in 1× PBS (pH 7.4), either 100 μg mL^{-1} or 1000 μg mL^{-1}, was introduced into the antibiotic inlet. 1, 2, 5 or 10 chambers were filled in the standard manner. Air was then used to push the antibiotic into the growth chamber. The bacteria metering chamber was then filled with the bacterial solution (12.5×10^6 cfu mL^{-1} *E. coli* in LB broth with 50 mM TBS pH 8.5 and 1 mM resazurin). Air was used to push this plug of fluid into the growth chamber where it diffusively mixed with the antibiotic. The chip was then incubated in a 37 °C water bath (to prevent evaporation) for 8 h.

Fluorescent image acquisition and analysis

A Luxeon Rebel Color LED (Green, LEDSupply) was used as a light source. A collimating lens was used to focus the light into a beam. This beam was passed through a plastic green filter (Roscolux) to remove any extraneous wavelengths and directed onto the growth chamber of the Digit Chip. Emitted light was passed through a 589 nm bandwidth filter (Edmund Optics) and imaged using a LG G3 cell phone camera equipped with an adhered PDMS lens.[35] Images were captured using the free Open Camera app and image analysis was performed using ImageJ. The red channel of the RGB image was extracted and the average intensity of the pixels in the growth chamber was measured. Each concentration of antibiotic was performed in triplicate and values were normalized to maximum and minimum pixel values, with error bars showing standard error.

Results and discussion

Overview of the Digit Chip

The Digit Chip consists of a series of chambers connected by capillary valves that serve as digitization elements (Fig. 1A). Upon manual application of a pressure *via* a button, the fluid bursts through the first capillary valve and enters the adjacent chamber (Fig. 1B). Through capillary pressure, the chamber fills spontaneously until the fluid reaches the subsequent capillary valve and the flow is arrested. The user can opt to fill the next chamber by re-pressing the button. The solution volume dispensed is programmed by the number of times the user applies pressure to the button.

The principle underlying the design of the device relies on the function of capillary valves created within the fluidic structure.[36] At the interface between the narrow and wide

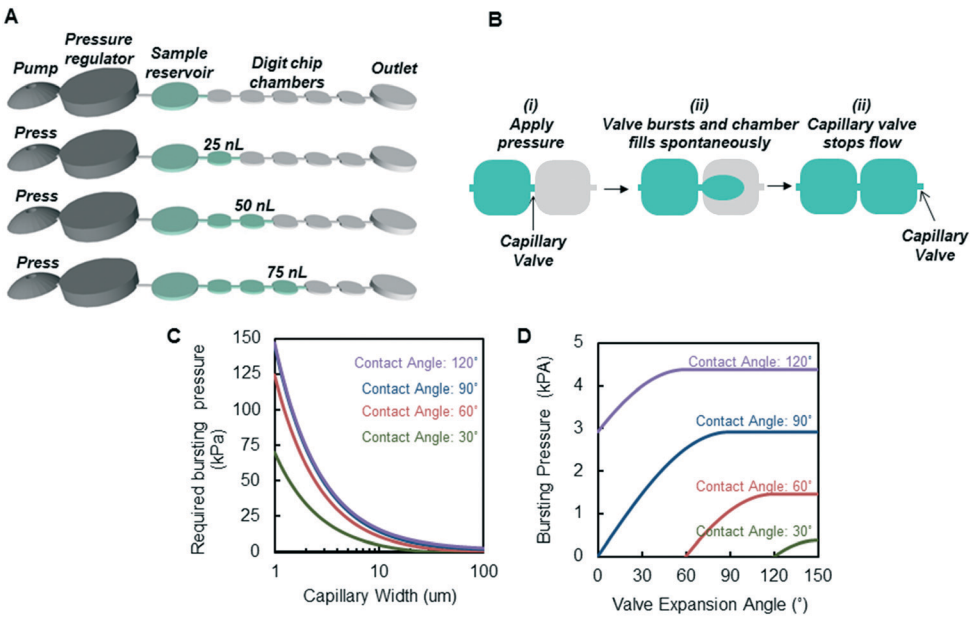

Fig. 1 Overview of the Digit Chip. (A) Schematic illustrating precise and user-programmable dispensing of ultra-low volumes using a Digit Chip. Chambers, which serve as the digital elements, are connected in series by capillary valves. After each button press, an additional chamber is filled with fluid. (B) A schematic illustrating the spontaneous filling of a chamber after pressure-induced bursting of a capillary valve. (C) Theoretical bursting pressure as a function of capillary valve width with a 90° valve expansion angle and 50 μm channel height. (D) Theoretical bursting pressure as a function of valve expansion angle for various contact angles assuming a 50 μm valve width and a 50 μm channel height.

regions, the liquid–air interface becomes pinned and requires a certain threshold pressure to resume movement. A valve exists between the narrow linear channel and the larger circular chamber, and the pressure is supplied by the press of a button. Once the valve bursts, the fluid will spontaneously fill the circular chamber. As long as the user only presses the button for a short period of time, the pressure is relieved before the fluid reaches the subsequent valve. As such, the pressure is below the critical pressure upon arrival at the next chamber, and motion ceases.

Bursting pressure model and design principles

Each valve must have a bursting pressure low enough that it can be readily applied by a human finger, but large enough that the valve does not burst spontaneously. To calculate the capillary valve bursting pressure, we use the following previously described equation for the maximum sustainable pressure across the meniscus in a rectangular configuration of the capillary burst valve:[36]

$$\Delta P = -2\sigma\left(\frac{\cos(\theta_I)}{w} + \frac{\cos(\theta_A)}{h}\right) \quad (1)$$

where ΔP is the pressure difference across the liquid–air interface, w is the valve width, h is the channel height, σ is the surface tension of the liquid–air interface (72.9 mN m^{-1}), θ_I is the contact angle with the initial side-wall prior to the expansion, and θ_A is the critical advancing contact angle.

Upon the application of pressure, the meniscus will bulge until the contact angle with the new sidewall after the valve reaches the critical advancing contact angle, θ_A. This occurs when $\theta_I = \theta_A + \beta$, where β is the valve expansion angle, or when θ_I is greater than 180°, the maximum sustainable contact angle.[36] Thus the valve will burst when θ_I equals the lower of $\theta_A + \beta$ or 180°. These equations assume that the fluid is dispensed from an infinite reservoir and do not consider the receding interface.

Using this equation, we modeled the bursting pressure as a function of valve width (Fig. 1C) and valve expansion angle (Fig. 1D) for a variety of contact angles. As expected, the bursting pressure increases with narrower valves and larger valve expansion angles. The calculations indicate that a valve expansion angle of approximately 90° or higher is optimal as the bursting pressure rapidly drops off for angles less than 90°. At low contact angles, the bursting pressure approaches zero for valve widths around 25 μm, thus valves narrower than 25 μm are ideal.

It is critical that the device surface be hydrophilic so that the chambers fill spontaneously *via* the capillary pressure after the valves burst. Thus, the contact angle of the fluid should be less than 90°. On the other hand, Fig. 1C and D suggest that at low contact angles, the valves will burst spontaneously for most valve widths and valve expansion angles. Thus, the surface should be engineered to be only slightly hydrophilic. We measured the critical advancing contact angle of PBS on PDMS for a variety of oxygen plasma treatment times (Fig. S1†). We found that with a 30 s oxygen plasma exposure, the contact angle of PBS on PDMS is 70° which is compatible with the Digit Chip. PDMS is a useful material for this device because of its compatibility with rapid prototyping. While its elastomeric properties are useful in the user interface, they are not essential for the functioning of the wells. The stability of PDMS surface chemistry was sufficient for our device to function properly within the same day of plasma treating. However, using different materials for the wells (*e.g.* glass) that have a more stable surface chemistry may be more advantageous if the device were to be mass-produced and stored for longer periods before use.

Optimization of device geometry

Motivated by these calculations, we fabricated an array of devices with various capillary valve widths and expansion angles to further refine the design. Devices were fabricated by pouring PDMS on a 50 μm tall SU-8 master mold patterned using standard photolithography. After curing, the PDMS was plasma treated and bonded to a glass substrate.

Fig. 2A shows the measured bursting pressure as a function of valve width and Fig. 2B shows the bursting pressure as a function of valve expansion angle. We compared our measured values to the theoretical predictions and in both cases, we find good agreement with the theory. In all of our designs, the channels connecting the wells were sufficiently short to ensure that there was not enough buildup of flow momentum between wells to break a capillary valve. Fig. 2C shows the bursting pressure as a function of the number of valves filled. On average, we observe only a 5% increase in bursting pressure after each sequential valve is filled.

We studied the accuracy of filling as a function of chamber size (Fig. 2D). A series of devices were designed with chamber diameters ranging from 55 μm to 800 μm and channel heights ranging from 5 μm to 50 μm tall. Since the capillary valve bursting pressure depends on the width of the valve and the expansion angle, the sizes of the circular chambers can be freely adjusted to allow for different volumes while performing in the same manner. The volume of these chambers ranged from approximately 21 pL to 24 nL. The valve widths scale with the chamber size and range from 2.5 to 20 μm wide. We found that all chambers and wells, including those as small as 21 pL, could be filled with at least 97% accuracy. The remaining chamber sizes filled with high accuracy (Fig. S2†). A small amount of error is caused by the incomplete filling of some chambers due to the occasional formation of small bubbles. However, the valves were stable, not spontaneously breaking even after many minutes. A small amount of evaporation does occur if the device is left unattended for a manner of minutes, but this does not destabilize the air–liquid interface.

This smallest dispensing volume achieved approaches the minimum achievable limit for our design, which we estimate to be 15–20 pL. The fabrication tolerance of our

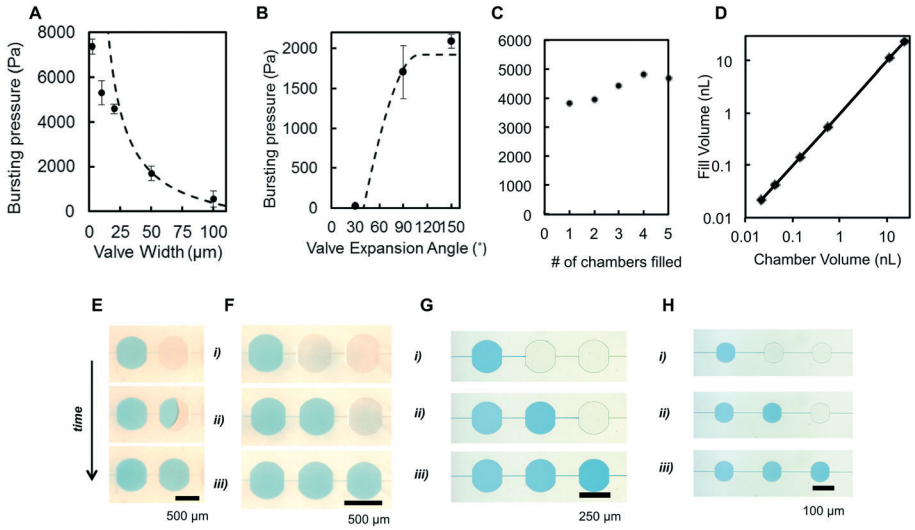

Fig. 2 Experimental investigation of the device geometry and its optimization. (A) Experimentally measured bursting pressure as a function of valve width. The dotted line represents the calculated bursting pressure assuming a 70° contact angle and 90° valve expansion angle. (B) Experimentally measured bursting pressure as a function of valve expansion angle. The dotted line represents the calculated bursting pressure assuming a 70° contact angle and 50 μm valve width. (C) The measured bursting pressure as sequential chambers are filled. (D) The measured volume dispensed as a function of chamber volume. (E) Images illustrating the spontaneous filling of a 12 nL chamber after the valve is burst by a user-applied pressure. Sequential dispensing of volumes in approximately (F) 12 nL, (G) 580 pL and (H) 140 pL increments. Errors bars represent standard error.

photolithography process creates minimum lateral sizes of the channel and chamber (to maintain the near 90° spreading angle). The valve design places an additional fundamental constraint on the valve aspect ratio, which limits how small the channel height can be. Since the free-energy barrier encountered at the side walls in the chamber opening must always exceed the favourable free-energy change associated with wetting the top and bottom walls, the width : height aspect ratio in the channels connecting the chambers must stay below a maximum value. This maximum aspect ratio is derivable from (eqn (1)) and given by:

$$\left[w/h\right]_{\max} = -\frac{\cos\left(\theta_A + \beta\right)}{\cos\left(\theta_A\right)} \tag{2}$$

A contact angle of 70° and a spreading angle (β) of 90°, gives a maximum aspect ratio is 2.75, limiting how small the channel height can be as a function of the width. This limit was in agreement with experiments showing that further reduction of the channel height for our smallest chamber size led to spontaneous breaking of the valves.

Designing a user-friendly interface

We sought to design an interface that allows the user to easily apply the appropriate pressure to break one capillary valve. The interface consists of two hollow PDMS chambers connected in series to the sample loaded in the Digit Chip (Fig. 3A and B). When the user fully compresses the first chamber, which serves as the button, the gas within the chamber is displaced and a pressure is applied to the sample in the Digit Chip. The applied pressure is regulated by tuning the size of the second pressure-regulation chamber. The pressure is vented through a small hole when the user releases the button.

The applied pressure difference generated by pressing the button can be approximated using Boyle's law:

$$\Delta P_{\text{applied}} = P_{\text{atm}}\left(\frac{V_b + V_s}{V_s} - 1\right) \tag{3}$$

where $\Delta P_{\text{applied}}$ is the applied pressure difference, P_{atm} is the atmospheric pressure of 101 325 Pa, V_b is the volume of the button chamber and V_s is the volume of the regulation chamber and the connective tubing. This equation assumes the button is fully compressed when pressed. This two-chamber design limits the maximum pressure a user can apply to the valve (achieved when the button is fully compressed) and therefore ensures that the user cannot press too hard.

We measured the applied pressure as a function of the ratio of the size of the button and pressure regulation chambers (Fig. 3C). The measured pressures are lower than the theoretical predictions (Fig. 3D), suggesting that the button chamber retains about 20% of its volume when fully depressed.

To test the efficacy of this interface, we connected various designs in series to a Digit Chip with 20 μm wide valves and 24 nL chambers. We measured the number of chambers filled per button press (Fig. 3E). We found that when using an interface with a ratio of the two chambers of 15%, we could accurately fill a single chamber per button press. The applied pressure from this interface design is 11 kPa, which

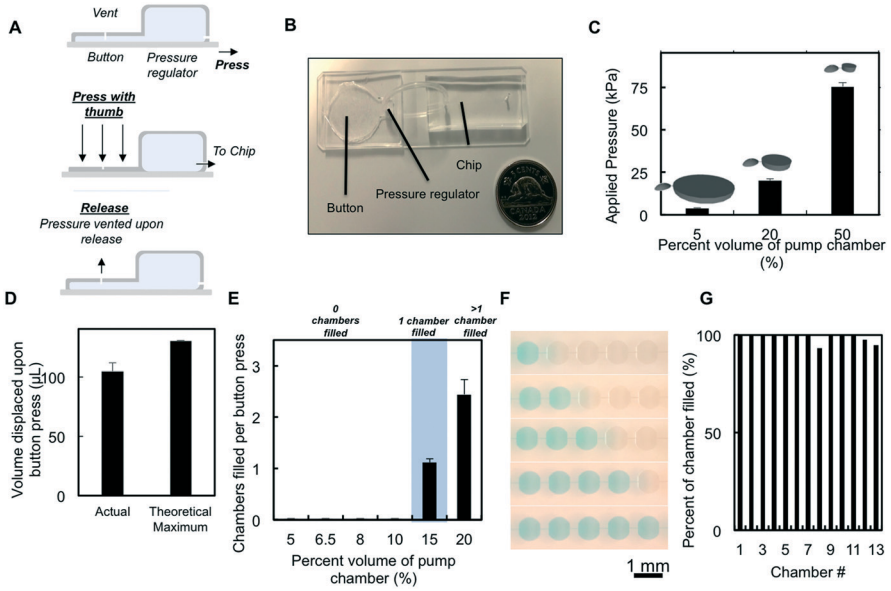

Fig. 3 The Digit Chip interface for controlled dispensing of droplets. (A) Schematic illustrating the user-friendly interface for precise application of pressure. The interface consists a button and a pressure regulation chamber patterned in PDMS. When the user depresses the button with a thumb-press, the applied pressure is controlled by the size of the pressure regulation chamber. Pressure is vented through a small hole when the user releases the button. (B) Image of the device with a nickel shown for scale. (C) The applied pressure as a function of the ratio of the size of the button and pressure regulation chambers. (D) Measurement of the volume displaced when the button is depressed. (E) The number of chambers filled as a function of the size of the pressure regulation chamber. Single chambers could be accurately filled when the button chamber was 15% the volume of the pressure regulator. (F) Images of solution dispensed in 24 nL increments using the PDMS button. (G) Accuracy of filling in 24 nL increments after each sequential button press using the user-interface. Solution was dispensed more than 10 times sequentially. Errors bars represent standard error.

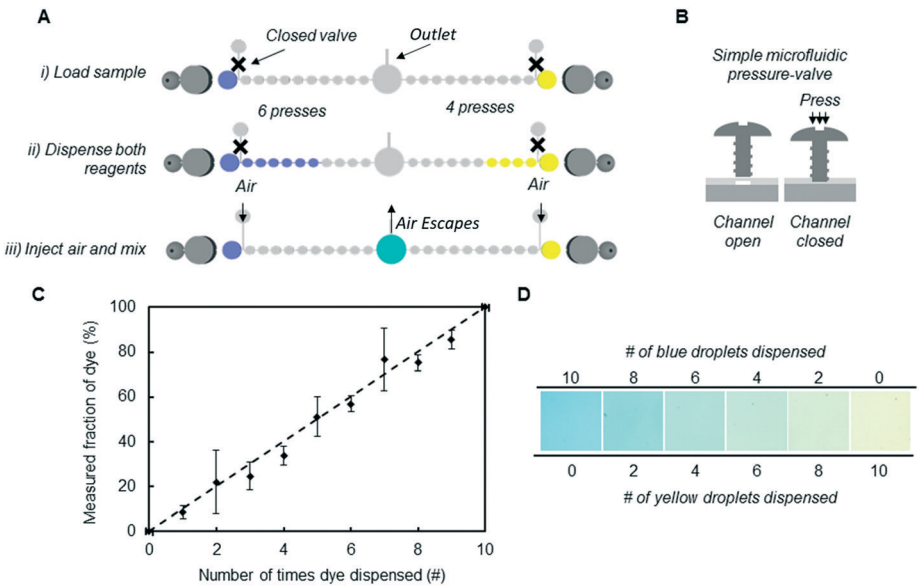

Fig. 4 Generation of a discretized concentration gradient. (A) Schematic illustrating on-chip dispensing and mixing of reagents using the Digit Chip. After the sample is loaded, both solutions are dispensed in various ratios in 24 nL increments. The two solutions were sent to a central mixing chamber by manually injecting air using a syringe. (B) Air channels were valved using a screw to depress the PDMS and block the channel. (C) On-chip generation of a discretized concentration gradient using the Digit Chip. Errors bars represent standard error. (D) Images acquired with an optical microscope after mixing the blue and yellow dye in various ratios with the Digit Chip.

is higher than the approximately 6 kPa capillary valve bursting pressure predicted by eqn (1). This is expected as the pressure generated by the user must be greater than the valve bursting pressure due to the pressure drop along the tubing, fluid reservoir, and channel and the fact that the flexible PDMS chambers expand under pressure. Fig. 3F shows images of dispensing fluid in 24 nL increments using this interface. Using the interface, we found that we could accurately dispense liquid in 24 nL increments over 10 times sequentially. The volume dispensed ranged from 24 nL for 1 button-

press to over 300 nL for 13 button-presses (Fig. 3G) and the chambers filled with over 98% filling accuracy and less than 3% standard deviation (Fig. 3G). The volumes dispensed in Fig. 2F–H were further replicated using the button to show its applicability to a variety of volumes (Fig. S3†).

Generation of a discrete concentration gradient

Concentration gradients and reagent dilutions are important in a variety of biological and chemical assays. As a demonstration that solutions can be accurately dispensed and combined, we used the Digit Chip to mix small solution volumes in precise ratios (Fig. 4A). In this device, two separate solutions can be dispensed up to 10 times in increments of 24 nL. After dispensing the liquid, the fluid is actuated towards the central mixing chamber by manually injecting air using a syringe. The air channels are closed during dispensing by screw valves,[37] which depress the channel (Fig. 4B).

We dispensed 10 different ratios of blue and yellow dyes in 24 nL increments and mixed the dyes in the central chamber on chip. For each concentration, the sum of the number of both droplets dispensed was kept constant at 10, corresponding to a total volume after mixing of 240 nL. Fig. 4C shows the measured ratios of the two solutions mixed on chip. The r^2 value of the fit to the line representing the expected ratio of the dyes is 0.98. The deviation in our measured values is due to the compounded error of filling 10 wells and the fact that some liquid remains trapped in the chambers after injecting air. Fig. 4D shows images of the resulting colors generated from mixing the two dyes.

A low-cost platform for rapid determination of bacterial antibiotic susceptibility

In order to demonstrate the usefulness of the Digit Chip for a practical application, a device was developed which tests the effect of antibiotic concentration on bacterial growth.[38] The chip is comprised of a pair of channels leading into a central growth chamber, each with a respective air inlet (Fig. 5A). A single outlet is present on the far side of the growth chamber. The top channel is the standard Digit Chip motif, with 10 chambers separated by capillary valves (Fig. 5A, i). By filling the desired number of chambers with antibiotic solution and expelling the metered antibiotic into the growth chamber, between 1 and 10 equivalents of antibiotic are introduced. The side channel is a single bacterial metering channel separated from the growth chamber by a capillary valve (Fig. 5A, ii). This chamber is filled with a fixed volume of bacterial solution, which can be transported by air into the growth chamber where it mixes diffusively with the antibiotic solution. This device can then be submerged in a 37° water bath to allow for bacterial growth.

To observe the viability of the bacteria, resazurin dye was added to the bacterial medium. Only in the presence of actively metabolizing bacteria will the resazurin be reduced to its fluorescently active product, resorufin. In order to measure the fluorescence of this product, a simple smart phone-based imaging platform was devised (Fig. 5B). The excitation system consists of a high-powered green LED light source, along with a collimating lens to focus the excitation light and a plastic green filter to remove extraneous wavelengths. This

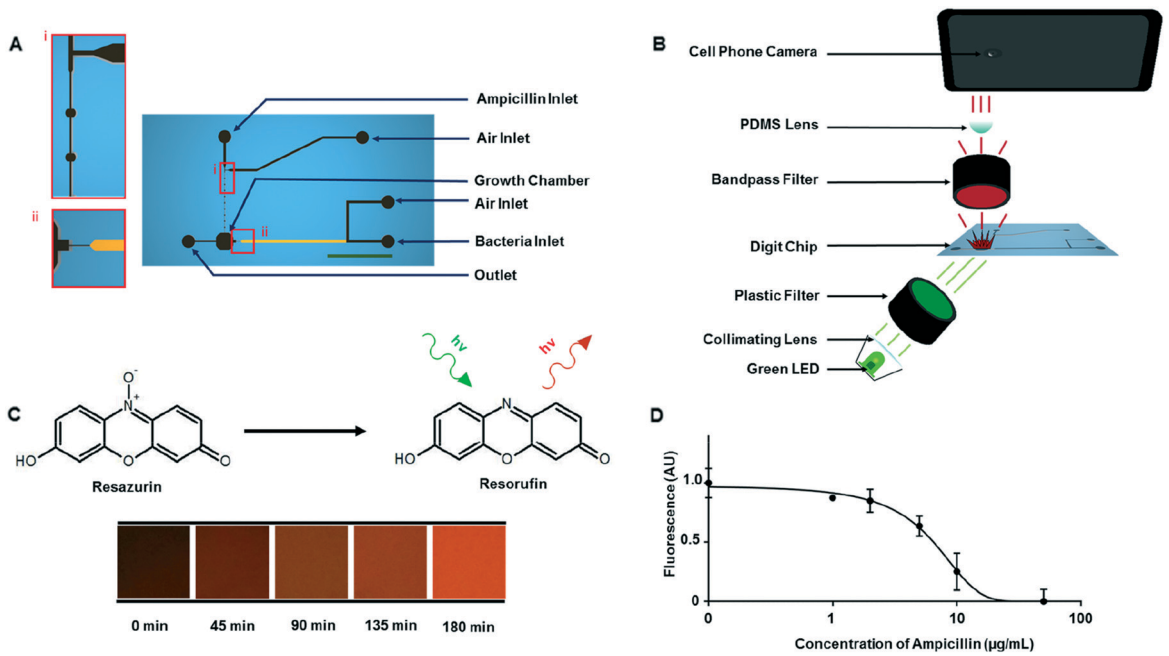

Fig. 5 Testing of antibiotic susceptibility. (A) Schematic illustrating architecture of device. Insets show Digit Chip motif (i) and capillary valve between bacterial metering channel (yellow) and growth chamber (ii). (B) Simple, smartphone-base fluorescence platform allowing for excitation with green light and imaging of resultant red fluorescence. (C) Time series demonstrating the conversion of non-fluorescent resazurin to highly fluorescent resorufin by bacterial metabolism. (D) Curve illustrating the effect of ampicillin titration on the viability of *E. coli*.

light is focussed onto the growth chamber of the chip from an oblique angle to minimize detection of the excitation light. The emitted light is passed through a 589 nm bandpass filter and imaged using an LG G3 smartphone camera. To magnify the image of the growth chamber, a PDMS lens was fabricated and affixed directly onto the back of the smartphone, covering the camera lens. The resultant RGB image was then split into its component red, green and blue channels, and the average intensity of the red channel was measured. In keeping with the intended use of the Digit Chip in low resource settings, the entire platform including all components can be purchased and constructed for under 60 USD.

In order to confirm the function of the platform, a high concentration (1.0×10^8) of bacteria was introduced into the growth chamber in the absence of antibiotic and the fluorescence was imaged every 45 minutes for 3 hours. The resultant images display monotonically increasing fluorescence as the bacteria replicate and metabolize (Fig. 5C). Evidently, the system is more than adequate for detecting the conversion of resazurin to resorufin and thereby measuring bacterial viability.

The susceptibility of *E. coli* to ampicillin was chosen as a suitable test case to confirm the efficacy of the Digit Chip. A wide range of concentrations (0, 1, 2, 5, 10 and 50 μg mL^{-1}) of antibiotic were introduced using the discretized measurement chambers and two stock solutions (100 μg mL^{-1} and 1000 μg mL^{-1}). These were mixed with bacterial solution (12.5×10^6 cfu mL^{-1}) and incubated for 8 h prior to measurement of fluorescence. The results are illustrated graphically in Fig. 5D. The graph follows a standard sigmoidal shape, with bacterial death beginning at a concentration of about 5 μg mL^{-1} and increasing until 50 μg mL^{-1}. These results are in good agreements with past studies, which have shown a minimum inhibitory concentration of 2 μg mL^{-1} [39] and complete inhibition of growth at 50 μg mL^{-1}.[40] Evidently, the ability of the Digit Chip to create titrations with a wide range of concentrations is ideally suited to investigating bacterial antibiotic susceptibility. Moreover, due to the extremely small volumes used (on the order of 100 nL) very small quantities of bacterial sample and antibiotic solution are required. This is particularly important in situations where the sample is limited by biological or financial constraints. Furthermore, this device is amenable to any combination of bacterial species and antibiotic, allowing for widespread implementation.

Discussion

This type of self-powered digital fluidic device may be useful for a wide class of assays in low-resource settings that require low sample or reagent volumes (*e.g.* pin-prick assays), or that require complex multi-step manipulations or precise timing that are difficult to automate using existing passive analog fluidics. Using this device, the user controls the time at which various reagents are introduced which eliminates the need for built-in timing mechanisms. This device is especially useful for assays in which the volumes dispensed are systematically varied, such as titrations. This device architecture is compatible with many common fabrication techniques currently used to make channel-based microfluidics at low cost.[41] As with other microfluidic technologies, the replacement of PDMS with more cost-effective alternatives (*e.g.* plastics, glasses) might also accompany the transition to larger-scale manufacturing.[41] For our device this would have the added benefit of enabling us to choose materials whose surface chemistry is more stable and suitable for long-term storage.

Along with these advantages, the Digit Chip does have some weaknesses. The nature of the capillary valve requires that metered fluid be displaced and replaced with air before the valve is re-established, meaning that the chambers need to be flushed with air between subsequent dispensings. Furthermore, valve dimensions need to be precise to allow for correct behaviour. However, these drawbacks are relatively minimal given the simplicity and accuracy of the device.

We applied the Digit Chip to evaluating antimicrobial resistance, which is an important target application to enable in resource-limited settings. The features of the Digit Chip would make it straightforward to carry out the type of drug titration that is typically used to assess whether a frontline antibiotic will be efficacious. This approach is also applicable to any of the multitude of tests in biology and chemistry that require titration. For example, the testing of dissociation constants and the activity of enzymes could be tested using minute quantities of reagents, provided that a measurable color change occurs.

The adoption of this technology in a wider variety of assays will also include its functioning with complex fluids, such as whole blood, that have a higher viscosity and contain suspended particles. Although the core principles of our device (*e.g.* eqn (1)) are independent of viscosity, whose only independent effect on our chips was to change the speed with which the chambers filled, the presence of suspended particles (*e.g.* blood cells) would place size restrictions on our chambers, with the smaller geometries having the capacity to become easily clogged.

Increasing the complexity of manipulations and involving more reagents in the Digit Chip would require more inlets, and a 2D configuration of these buttons and valves. Valving mechanisms must be added at each node to control the directionality of pressure applied, just as was illustrated here to make the concentration gradient. One natural extension of the existing device would be to have two parallel Digit Chip motifs emptying into a common chamber, with one having chambers 10× larger than the other. This "ones and tens" configuration would allow any integer value between 1 and 100 to be metered and dispensed with only a small increase in complexity.

Just as has been shown with digital microfluidics,[21–23] a vast modular library of manipulations and different assays could be built from the Digit Chip using a few stock 1D and 2D configurations of wells, valves and buttons. These device configurations would need to be optimized for the maximum number and type of fluid manipulations possible, but not with a need for any reagents to be loaded beforehand. Therefore a single chip design could be used for many assays (*e.g.* any titration involving a given number of reagents) or rapid

experiments performed in the field. However, this modularity comes at the cost of easy assay automation. A general limitation of user-programmable digital fluidic platforms is that more sophisticated assays may require more buttons and thus, greater user involvement and more complicated instructions.

Conclusion

In summary, we introduce a device for power-free and user-programmable manipulation of small sample volumes. A sequence of microfluidic chambers connected by capillary valves connected to pressure-regulated buttons allow for discretized dispensing of sub-nanoliter volumes. This device architecture enabled power-free dispensing of volumes in increments as low as 21 pL and near 97% accuracy. The volume dispensed could be fine-tuned in 10 increments across one order-of-magnitude. The number of volume increments could be increased in future iterations of the device. A series of devices is used to generate a concentration gradient with 10 discrete concentrations in sub-microliter volumes, and to determine the susceptibility of bacteria to various concentrations of antibiotic. This device could help bring a new class of assays, which require sophisticated manipulations of small volumes, to low-resource settings.

Acknowledgements

This work was funded by the Government of Canada through Genome Canada and the Ontario Genomics Institute (OGI-077) and the Ontario Research Fund administered by the Ministry of Research and Innovation of Ontario. We thank ECTI facility at the University of Toronto for use of the cleanroom facilities. J. D. B. acknowledges support from an Ontario Graduate Scholarship. I. B. B. acknowledges the Natural Sciences and Engineering Research Council of Canada for a Banting Fellowship.

Notes and references

1 P. Yager, T. Edwards, E. Fu, K. Helton, K. Nelson, M. R. Tam and B. H. Weigl, *Nature*, 2006, **442**, 412–418.
2 S. O. Kelley, C. A. Mirkin, D. R. Walt, R. F. Ismagilov, M. Toner and E. H. Sargent, *Nat. Nanotechnol.*, 2014, **9**, 969–980.
3 B. Lutz, T. Liang, E. Fu, S. Ramachandran, P. Kauffman and P. Yager, *Lab Chip*, 2013, **13**, 2840–2847.
4 C. Renault, J. Koehne, A. J. Ricco and R. M. Crooks, *Langmuir*, 2014, **30**, 7030–7036.
5 H. Liu and R. M. Crooks, *J. Am. Chem. Soc.*, 2011, **133**, 17564–17566.
6 T. Laksanasopin, T. W. Guo, S. Nayak, A. A. Sridhara, S. Xie, O. O. Olowookere, P. Cadinu, F. Meng, N. H. Chee, J. Kim, C. D. Chin, E. Munyazesa, P. Mugwaneza, A. J. Rai, V. Mugisha, A. R. Castro, D. Steinmiller, V. Linder, J. E. Justman, S. Nsanzimana and S. K. Sia, *Sci. Transl. Med.*, 2015, **7**, 273re1.
7 I. K. Dimov, L. Basabe-Desmonts, J. L. Garcia-Cordero, B. M. Ross, A. J. Ricco and L. P. Lee, *Lab Chip*, 2011, **11**, 845–850.
8 M. M. Gong, B. D. MacDonald, T. Vu Nguyen and D. Sinton, *Biomicrofluidics*, 2012, **6**, 044102.
9 S. Begolo, D. V. Zhukov, D. A. Selck, L. Li and R. F. Ismagilov, *Lab Chip*, 2014, **14**, 4616–4628.
10 R. Safavieh, G. Z. Zhou and D. Juncker, *Lab Chip*, 2011, **11**, 2618–2624.
11 R. Safavieh and D. Juncker, *Lab Chip*, 2013, **13**, 4180–4189.
12 R. Safavieh, A. Tamayol and D. Juncker, *Microfluid. Nanofluid.*, 2014, **18**, 357–366.
13 A. K. Yetisen, M. S. Akram and C. R. Lowe, *Lab Chip*, 2013, **13**, 2210–2251.
14 N. K. Thom, G. G. Lewis, K. Yeung and S. T. Phillips, *RSC Adv.*, 2014, **4**, 1334–1340.
15 M. Funes-Huacca, A. Wu, E. Szepesvari, P. Rajendran, N. Kwan-Wong, A. Razgulin, Y. Shen, J. Kagira, R. Campbell and R. Derda, *Lab Chip*, 2012, **12**, 4269–4278.
16 F. Deiss, M. E. Funes-Huacca, J. Bal, K. F. Tjhung and R. Derda, *Lab Chip*, 2014, **14**, 167–171.
17 L. Luo, X. Li and R. M. Crooks, *Anal. Chem.*, 2014, **86**, 12390–12397.
18 M. T. Guo, A. Rotem, J. A. Heyman and D. A. Weitz, *Lab Chip*, 2012, **12**, 2146–2155.
19 L. Rosenfeld, T. Lin, R. Derda and S. K. Y. Tang, *Microfluid. Nanofluid.*, 2014, **16**, 921–939.
20 M. Kim, M. Pan, Y. Gai, S. Pang, C. Han, C. Yang and S. K. Y. Tang, *Lab Chip*, 2015, **15**, 1417–1423.
21 A. H. C. Ng, M. D. Chamberlain, H. Situ, V. Lee and A. R. Wheeler, *Nat. Commun.*, 2015, **6**, 1–12.
22 I. A. Eydelnant, B. Betty Li and A. R. Wheeler, *Nat. Commun.*, 2014, **5**, 1–9.
23 D. Witters, K. Knez, F. Ceyssens, R. Puers and J. Lammertyn, *Lab Chip*, 2013, **13**, 2047–2054.
24 A. Puntambekar, J.-W. Choi, C. H. Ahn, S. Kim and V. Makhijani, *Lab Chip*, 2002, **2**, 213–218.
25 M. Hitzbleck, L. Avrain, V. Smekens, R. D. Lovchik, P. Mertens and E. Delamarche, *Lab Chip*, 2012, **12**, 1972–1978.
26 K. Iwai, K. C. Shih, X. Lin, T. A. Brubaker, R. D. Sochol and L. Lin, *Lab Chip*, 2014, **14**, 3790–3799.
27 F. Shen, B. Sun, J. E. Kreutz, E. K. Davydova, W. Du, P. L. Reddy, L. J. Joseph and R. F. Ismagilov, *J. Am. Chem. Soc.*, 2011, **133**, 17705–17712.
28 F. Shen, W. Du, E. K. Davydova, M. A. Karymov, J. Pandey and R. F. Ismagilov, *Anal. Chem.*, 2010, **82**, 4606–4612.
29 R. R. Pompano, C. E. Platt, M. A. Karymov and R. F. Ismagilov, *Langmuir*, 2012, **28**, 1931–1941.
30 H. Liu, X. Li and R. M. Crooks, *Anal. Chem.*, 2013, **85**, 4263–4267.
31 W. Li, T. Chen, Z. Chen, P. Fei, Z. Yu, Y. Pang and Y. Huang, *Lab Chip*, 2012, **12**, 1587–1590.
32 K. Xu, M. R. Begley and J. P. Landers, *Lab Chip*, 2015, **15**, 867–876.
33 J. Leng and J.-B. Salmon, *Lab Chip*, 2009, **9**, 24–34.
34 N. Li Jeon, H. Baskaran, S. K. W. Dertinger, G. M. Whitesides, L. Van de Water and M. Toner, *Nat. Biotechnol.*, 2002, **20**, 826–830.
35 Y. Sung, J. Jeang, C. Lee and W. Shih, *J. Biomed. Opt.*, 2015, **20**, 047005.

36 H. Cho, H. Y. Kim, J. Y. Kang and T. S. Kim, *J. Colloid Interface Sci.*, 2007, **306**, 379–385.
37 S. E. Hulme, S. S. Shevkoplyas and G. M. Whitesides, *Lab Chip*, 2009, **9**, 79–86.
38 N. J. Cira, J. Y. Ho, M. E. Dueck and D. B. Weibel, *Lab Chip*, 2012, **12**, 1052–1059.
39 D. Greenwood and F. O'Grady, *J. Med. Microbiol.*, 1969, **2**, 435–441.
40 M. Kitagawa, T. Ara, M. Arifuzzaman, T. Ioka-Nakamichi, E. Inamoto, H. Toyonaga and H. Mori, *DNA Res.*, 2006, **12**, 291–299.
41 C. D. Chin, V. Linder and S. K. Sia, *Lab Chip*, 2012, **12**, 2118–2134.